

Steric Molecular Combing Effect Enables Ultrafast Self-Healing Electrolyte in Quasi-Solid-State Zinc-Ion Batteries

Qin Liu, Renpeng Chen, Lin Xu,* Yu Liu, Yuhang Dai, Meng Huang, and Liqiang Mai*

Cite This: *ACS Energy Lett.* 2022, 7, 2825–2832

Read Online

ACCESS |



Metrics & More

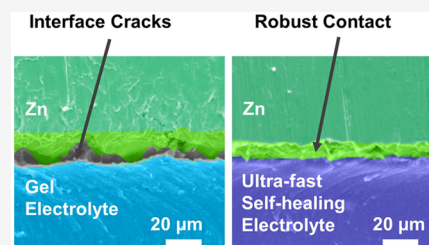


Article Recommendations



Supporting Information

ABSTRACT: Quasi-solid-state Zn metal batteries show great potential for next-generation batteries due to their inherent safety and high energy density. However, the mismatch between the static quasi-solid electrolyte surface and the dynamic Zn anode volume change will lead to inferior interfacial contact, which severely hinders the development of Zn-based batteries. Herein, a unique steric molecular combing strategy is proposed to design an ultrafast self-healing electrolyte for constructing a dynamically self-adaptive interface. Theoretical simulations and experimental characterizations reveal the steric molecular combing effect, which combs and straightens the guar gum molecular chain by inhibiting the intramolecular rotation. Concomitantly, the stretched molecular chain exposes more alcoholic hydroxyl active sites, enabling rapid dynamic cross-linking for ultrafast self-healing electrolytes. Consequently, the full battery shows an ultralong cycling lifespan of 10000 cycles with 98.5% capacity retention, and stable Zn stripping/plating is achieved at 10 mA cm^{-2} and 10 mAh cm^{-2} , respectively, pushing forward the next-generation high-performance zinc-ion battery.



Art water, the latest popular children's toy, has several intriguing properties, such as shape adaptability, high viscoelasticity, and reusability (Figure S1a). It is also called "fake water" due to its highly similar appearance to water, which is actually a sort of hydrogel. This attractive shape-adaptive behavior is attributed to its dynamic cross-linking.^{1,2} These dynamic cross-linking bonds form the matrix of art water, which can tie the guar gum chains to lock the shape temporarily. When the substance is subjected to an external impact, the dynamic bonds will be broken and then reform again at a different location, explaining its nature of high shape adaptability.^{3,4} In particular, it can heal spontaneously once it receives external damage such as an external puncture.⁵ Due to their exceptional advantages, such dynamic intelligent materials perform an inspiring role in up and coming fields such as soft robotics,^{6,7} biomedical engineering, and 3D printing.^{8,9} This exclusive shape-adaptive performance makes the substance totally different from the published traditional gel electrolyte and the artificial interface layer of the battery.¹⁰

Herein, we propose a concept for applying modified quasi-solid-state "art water" with highly self-adaptive behavior to zinc-ion batteries as electrolytes for the first time. Quasi-solid-state zinc-ion batteries are perceived as the most promising candidates for the forthcoming wearable electronic products due to the unique advantages of Zn metal, including high volumetric capacity (5854 Ah L^{-1}), abundant resources in the Earth's crust, and facile manufacturing.^{11,12} Equally impor-

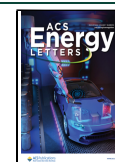
tantly, it avoids the use of aqueous electrolytes that lead to irreversible reactions, including parasitic hydrogen evolution reaction (HER), zinc corrosion, and irreversible byproducts,^{13–15} which will severely deteriorate the cell performance of zinc-ion batteries. Therefore, it is believed that a gel electrolyte will pave the way for an anticorrosion and highly stable Zn anode. However, the development of quasi-solid-state zinc-ion batteries has been plagued by severe interfacial issues. During cycling, the Zn metal anode will inevitably develop some "hot spots" originating from uneven ion diffusion and deposition (Figure S1b),^{16,17} where the Zn plating/stripping rate is higher than that at other positions, resulting in the differential dynamic expansion of the zinc anode.^{18–20} Unfortunately, the static quasi-solid electrolyte surface cannot match the dynamic Zn anode, which will lead to an initial tight interface into a semicontinuous state after deep charge/discharge cycling and ultimately a premature failure of the battery.^{21–23}

In recent years, considerable efforts have been devoted to addressing the interfacial issue.^{24–27} A promising strategy is

Received: June 27, 2022

Accepted: July 29, 2022

Published: August 3, 2022



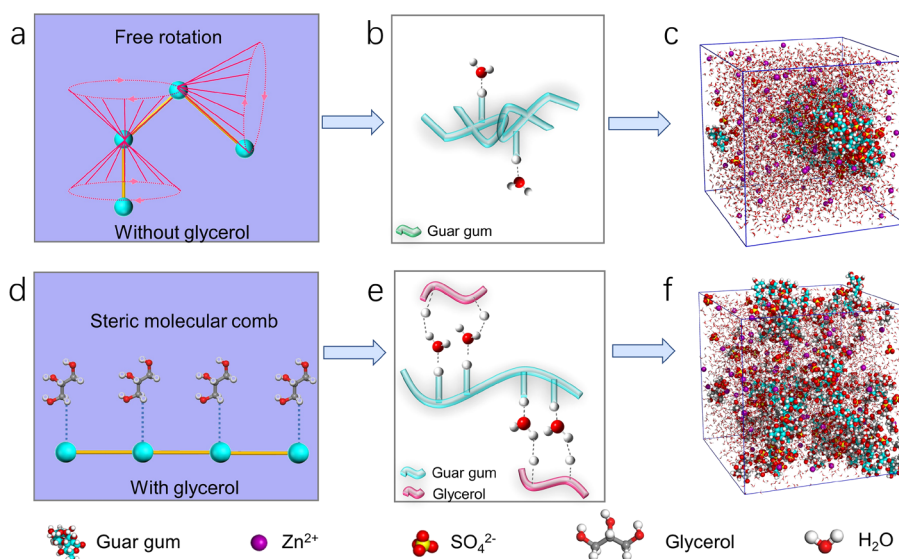


Figure 1. Steric molecular combing effect for guar gum molecular conformation regulation. (a, b) Schematic illustrations of intramolecular rotation and self-crimping of guar gum molecules. (c) 3D snapshot of the guar gum/ ZnSO_4 system obtained from MD simulations. (d, e) Schematic illustrations of the steric molecular combing effect for stretching guar gum molecules with glycerol. (f) 3D snapshot of the guar gum/ ZnSO_4 /glycerol system obtained from MD simulations.

establishing *in situ* solid electrolyte interphase via cation solvation regulation;²⁸ However, because of the high charge density of Zn^{2+} and the low dissociation degree of Zn salt in a wide concentration range, this leads to the limited modulation of the interfacial stability and low reversibility of the zinc anode. In addition, a rigid solid electrolyte provides an effective tactic to stabilize the Zn metal anode, due to its high mechanical strength and anhydrous properties.²⁹ Unfortunately, most solid electrolytes encounter low ionic conductivity problems,^{30–32} resulting in sluggish Zn^{2+} diffusion kinetics, low discharge capacity, and poor cycle lifespan. Moreover, the rigid surface also cannot maintain a conformal contact with the Zn metal anode during the dynamic plating/stripping process at a microscale level.³³ Therefore, the interfacial issue is still a major obstacle in developing advanced ZIBs with long cycle life. Thus, it is meaningful to construct a close interface to suppress Zn-dendrite-induced microvoids through dynamic self-healing electrolytes to achieve a dendrite-free zinc anode.

In this work, inspired by the interesting self-adaptive “art water”, we demonstrate a steric molecular combing effect to construct an ultrafast self-healing guar gum based electrolyte for dynamically adaptive interfaces. Art-water solidification is a critical point for its application in quasi-solid-state zinc-ion batteries. However, the challenge is that guar gum in “art water” is confronted with severe self-crimping and agglomeration issues, leading to low dispersion and poor mechanical strength. With these issues in mind, we innovatively introduced glycerol into the guar gum system to build a steric molecular comb. Specifically, glycerol is adsorbed on the guar gum molecular chains through hydrogen-bonding interactions, inhibiting the rotation of the carbon–carbon single bond, thereby combing and straightening the molecular chain. The resultant exposed alcoholic hydroxyl active sites can be dynamically cross-linked with borate to achieve an ultrafast self-healing capability. In addition, the electrolyte has a stronger binding energy with active water molecules in the system, reducing the number of water molecules in the primary solvation shell of Zn^{2+} from 6 to 3.8. Due to the two crucial

functions of the electrolyte above, the $\text{Zn}||\text{Zn}$ symmetrical cells exhibit a long-term durability over 400 h at a high current density (10 mA cm^{-2}) and a high cycling capacity (10 mAh cm^{-2}) and the quasi-solid-state full battery displays a 10000-cycle life with a capacity retention of 98.5%. This work presents a novel and effective method to solve the solid/solid interface issues by constructing a dynamic and self-adaptive interface. Hence, this pioneering design provides new insight into the challenges of solid/solid interfacial issues for constructing long-lifespan quasi-solid-state Zn metal batteries.

The molecular conformations of guar gum molecular chains in different systems are schematically illustrated in Figure 1. The spontaneous free rotation of the carbon–carbon single bond of the guar gum molecular chain will lead to irregular curling (Figure 1a). Coiled macromolecules, with enhanced hydrogen-bonding interactions, usually exhibit an aggregation state. Concomitantly, most of the active alcohol hydroxyl sites on the main chain are shielded, and the resulting guar gum based electrolyte displays an inferior self-healing ability at high concentrations (Figure 1b), which limits its application in quasi-solid-state Zn-ion batteries. To solve this issue, we developed a three-step synthetic procedure to straighten the guar gum molecular chains. First, glycerol was added to a 1 M ZnSO_4 solution to form a binary solvent system. The optimal content of glycerol is given in Experimental Section. Second, we dissolved guar gum completely in the as-prepared colloid to create a uniform solution. Glycerol is linked to the main chain by hydrogen bonds to form a steric molecular comb (Figure 1d), which can effectively regulate the molecular conformation of guar gum from a random coil state to a straight molecular chain state (Figure 1e). Finally, a neutral organoboron compound was introduced to cross-link the polymer chain and solidify it to obtain a porous network (Figures S1c and S2) with ultrafast self-healing and outstanding mechanical properties.

Molecular dynamics (MD) simulations were carried out to reveal the steric molecular combing mechanism in the guar gum/ ZnSO_4 and guar gum/ ZnSO_4 /glycerol systems, respec-

tively. A simulated system conformation shows that guar gum molecules are in an aggregated state and have strong interactions with surrounding sulfate molecules in the guar gum/ ZnSO_4 system (Figure 1c). In contrast, the guar gum molecules are uniformly dispersed in the guar gum/ ZnSO_4 /glycerol system, and the sulfate radicals are also homogeneously distributed into the solution (Figure 1f). This result suggests that steric molecular combing can inhibit molecular agglomeration and straighten molecular chains, which is consistent with the experimental results (Figure S3). Additionally, a single 3D snapshot of guar gum molecules in guar gum/ ZnSO_4 /glycerol exhibits more hydroxyl active sites in comparison to the guar gum/ ZnSO_4 system (Figure S4), which reveals the intrinsic reason for the ultrafast self-healing capability.

To visualize the self-adaptive interface directly, we simulated the microscopic changes of the electrolyte during the growth of dendrites through a tip experiment, as shown in Figure 2. A

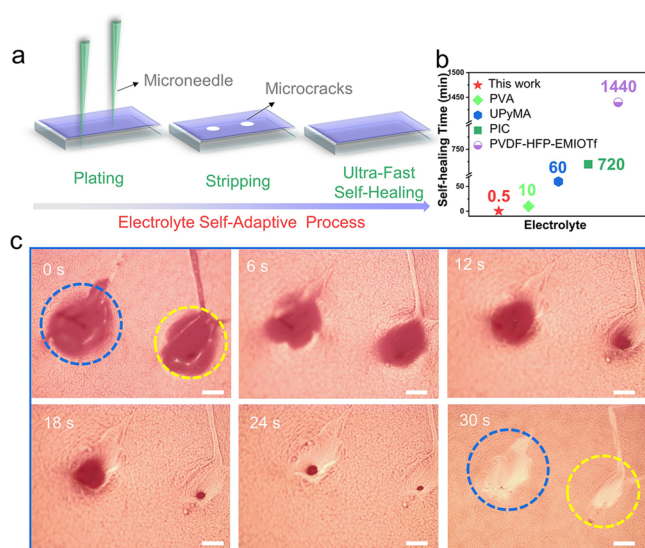


Figure 2. Steric molecular combing effect for ultrafast self-healing and self-adaptive electrolytes. (a) Schematic diagram of needle tip simulation experiment. (b) Self-healing time of our polymer electrolyte in comparison with those of previously reported self-healing electrolytes. (c) Optical images for the self-healing process after the needle tip is removed. Scale bars: 10 μm .

needle tip with a diameter of 20 μm was used to pierce the electrolyte to simulate the electrochemical behavior of the Zn dendrites after deep charge/discharge (Figure 2a). In a typical discharge process, the Zn dendrites shrink, corresponding to the stripping process. As seen through an optical microscope, the electrolyte scratch gradually heals after the needle tip is removed, as shown in Figure 2c and Figure S5. The tip removal process can be regarded as a dendrite dissolution process. The damaged area of the electrolyte interface gradually heals and returns to a flat surface within 30 s. This indicates that the electrolyte can achieve autonomous and rapid self-healing under air conditions without any external stimulation, which plays a vital role in building a strong and dynamic solid–solid interface contact and inhibiting the growth of Zn dendrites. The self-healing capacity (0.5 min) at room temperature dramatically surpasses those of previously reported advanced self-healing electrolytes (Figure 2b), such as PVA/ $\text{Zn}(\text{CF}_3\text{SO}_3)_2$ hydrogels (10 min),³⁴ polyion-complex

(PIC) hydrogels (720 min),³⁵ PVDF-co-HFP-5545 polymer (1440 min),³⁶ and UPyMA-PETE copolymer (60 min).³⁷

To further demonstrate the self-healing property, the macroscopic characteristics were determined (Figure S6). We cut the as-prepared gel electrolyte with and without piro red into small pieces with a scalpel. With the piro red stain available, the fresh cut interface will be clear rather than just a general fuzzy area. When two pieces of guar gum hydrogel come into contact with each other, electrolytes quickly merge into one within 30 s, further suggesting the superiority of the steric molecular combing effect. The formation kinetics of the borate bond is very rapid, generally considered to be 0.33 s,^{38,39} and with the extension of the self-healing time, the system gradually reaches equilibrium and eventually achieves complete self-healing. Fourier transform infrared spectroscopy (FT-IR) was then used to investigate the enhanced steric molecular combing mechanism for the as-prepared electrolyte. As presented in Figure S7, the guar gum powder shows a broad band at 3409 cm^{-1} , which is attributed to the O–H stretching vibrations. The apparent band at 1600 cm^{-1} corresponds to the hydroxyl bending. The bands at 2906 (C–H stretching vibrations), 1405 (C–H bending vibration), and 1150 cm^{-1} (C–O–C stretching vibration) are typical absorption bands of guar gum. In the guar gum/ ZnSO_4 system, the spectrum of the $\text{B}(\text{OH})^{4-}$ cross-linked guar gum electrolyte exhibits an absorption band at 1312 cm^{-1} , which is associated with a B–O stretching vibration. The formation of the B–O dynamic covalent bond reveals the intrinsic reason for the self-healing performance and proves the successful cross-linking of the borate ion ($\text{B}(\text{OH})^{4-}$) and the hydroxyl group. When glycerol was introduced as the second cross-linking network, the bands at 1413 and 1109 cm^{-1} were associated with a CH_2 bending vibration and C–O asymmetrical stretching vibration, respectively. The apparent bands at 1043 and 993 cm^{-1} are characteristic signals of symmetrical stretching vibration of a primary alcohol, which confirms the successful preparation of the binary-system gel. It is worth noting that the B–O peaks were intensified, demonstrating that more covalent bonds could be built between guar gum and $\text{B}(\text{OH})^{4-}$. This further proved that the steric molecular combing effect could effectively expose more alcoholic hydroxyl active sites directly and thus enhance the self-healing capability.

In addition to the excellent self-healing properties, the steric molecular combing effect also regulates the first solvation structure of Zn^{2+} ions. The average coordination number (ACN) in the primary solvation shell was then calculated (Figure 3a). In 1 M ZnSO_4 electrolyte, the ACN of Zn–O (H_2O) in the first hydration layer is around 6, while the ACNs of Zn–O (H_2O) in the first hydration layer under guar gum/ ZnSO_4 system and guar gum/ ZnSO_4 /glycerol system are around 4.7 and 3.8, respectively. The reduced ACN confirmed that the binary system could modulate the coordination of H_2O molecules with Zn^{2+} inside the primary solvation shell, which suggests the reduced number of active water molecules in the system. The modulation of the coordination structure of Zn^{2+} is attributed to the large quantity of active sites exposed by the steric molecular combing effect, which can immobilize water molecules. This conclusion was further supported by subsequent density functional theory (DFT) calculations.⁶⁷ ^{67}Zn nuclear magnetic resonance (NMR) spectroscopy also shows that the Zn^{2+} solvation sheath in the guar gum/ ZnSO_4 /glycerol system has fewer H_2O molecules (Figure 3b). The ^{67}Zn peak shifts higher to 6.7 ppm, indicating the reduced

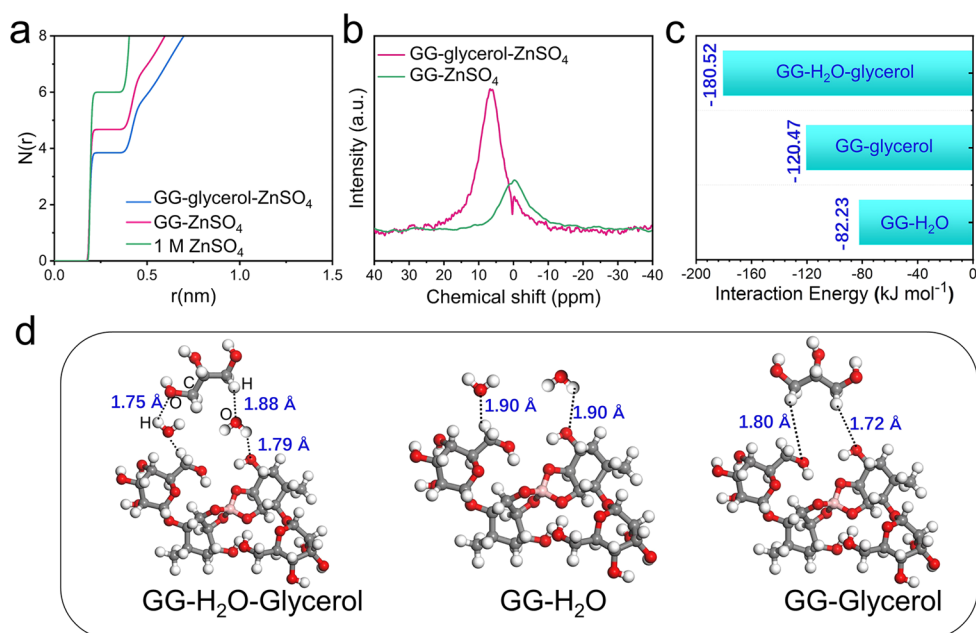


Figure 3. Steric molecular combing effect for solvated structure modulation of Zn^{2+} ions. (a) Coordination number between Zn^{2+} and O (H_2O). (b) ^{67}Zn nuclear magnetic resonance (NMR) spectra in the guar gum/ ZnSO_4 /glycerol and guar gum/ ZnSO_4 systems. (c, d) Density functional theory (DFT) optimized structures of guar gum (GG) in different systems and the corresponding interaction energies.

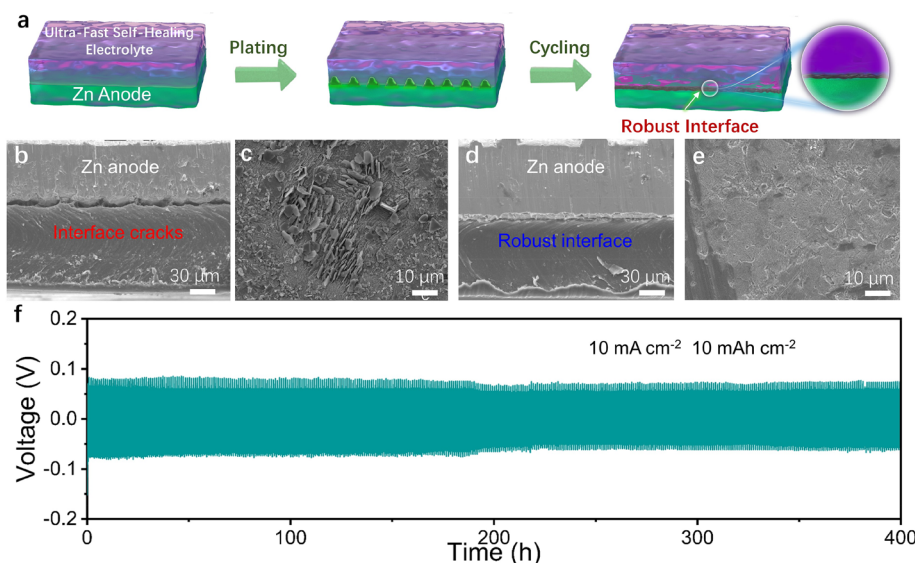


Figure 4. Characterizations of self-healing and self-adaptive interface. (a) Schematic diagram of the dendrite inhibition. (b, c) SEM images of Zn anodes after 250 cycles in the guar gum/ ZnSO_4 electrolyte. (d, e) SEM images of Zn anodes after 250 cycles in guar gum/ ZnSO_4 /glycerol electrolyte. (f) Symmetric cycling performance of Zn||Zn cells using guar gum/ ZnSO_4 /glycerol electrolyte at 10 mA cm^{-2} and 10 mAh cm^{-2} .

electron cloud density around the Zn^{2+} . NMR results showed an excellent agreement with MD simulations for the lower ACN in the guar gum/ ZnSO_4 /glycerol system.

Density functional theory (DFT) calculations were performed to gain a further understanding of the pivotal role of the binary solvent in the gel electrolyte (Figure 3c,d). A DFT analysis indicates that the hydrogen bonds in the glycerol/water binary system are more stable than those in the guar gum/ ZnSO_4 system (Figure S8), and the guar gum/ ZnSO_4 /glycerol system exhibits the largest interaction energy ($180.52 \text{ kJ mol}^{-1}$) (Figure 3c), demonstrating that the glycerol–water binary system can form a more robust network in comparison to pure glycerol or water, which is vital to

immobilize free H_2O molecules in the system and reduce the coordination number of H_2O molecules in the solvation shell of Zn^{2+} . In combination with the previous MD simulations, the active sites exposed by the steric molecular combing effect and their large binding energy with water molecules realize the solvated structure modulation of Zn^{2+} ions. In addition, the large binding energy with water molecules is beneficial to improve the water-locking capacity of the gel (Figure S9).

Those aforementioned advantages and properties of the binary-system gel make it an ideal electrolyte for quasi-solid-state Zn-ion batteries. The proposed schematic illustrations of interfacial issues are graphically depicted in Figure 4a and Figure S10. In a typical discharge/charge cycle of Zn-ion

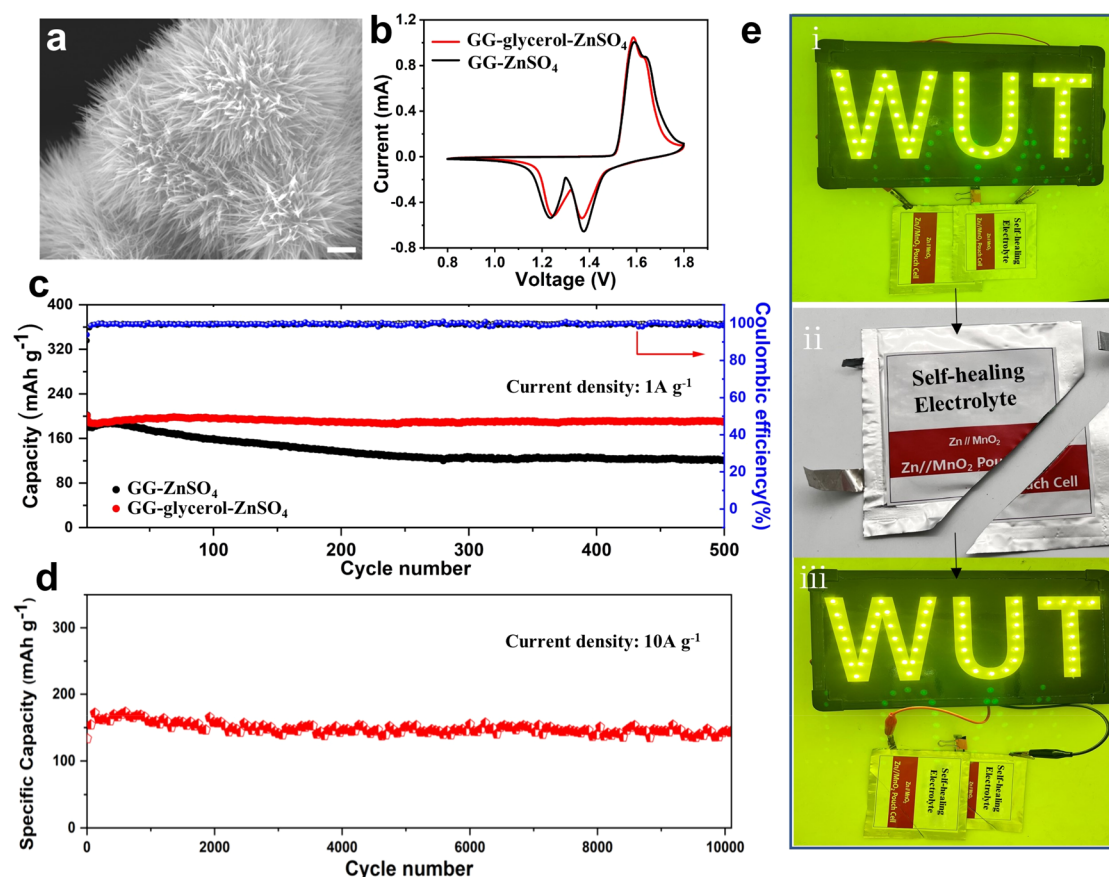


Figure 5. Electrochemical performance of zinc-ion full batteries with a self-adaptive interface. (a) SEM image of the MnO_2 cathode material. (b) CV curves of the full batteries in guar gum/ ZnSO_4 /glycerol and gum/ ZnSO_4 electrolytes. (c) Long-term cycling performance at 1 A g^{-1} . (d) Long-term cycling performance at 10 A g^{-1} . (e) Photographs of self-healing pouch cells powering a LED device: (i) before cutting; (ii) cutting off; (iii) after self-healing.

batteries, Zn dendrites will dynamically deposit and dissolve on the Zn anode, accompanied by a severe volume expansion and contraction. After a long-term cycling process, the Zn anodes will gradually thicken due to the apparent cumulative effect and inhomogeneous dendrite deterioration,²¹ which will make the interface contact between the quasi-solid electrolyte and the Zn anode electrode semicontinuous (Figure S10). The ultrafast self-healing and self-adapting capability keep the electrolyte and Zn anode interface dynamic and enable a robust contact during repeated Zn plating/stripping cycles (Figure 4a). Specifically, the self-healing electrolyte will spontaneously return to a flat state with the gradual dissolution of dendrites. Thus, the interface always remains in close and effective contact, facilitating the smooth, stable, and dense deposition of Zn metal.

In order to verify our conjecture, the morphology of the Zn electrode and the interface after 250 cycles at a current density of 1 mA cm^{-2} in the guar gum/ ZnSO_4 and guar gum/ ZnSO_4 /glycerol systems were examined respectively by scanning electron microscope (SEM). Obviously, there are enormous cracks between the Zn anode electrode and the quasi-solid-state electrolyte in the guar gum/ ZnSO_4 system after cycling (Figure 4b). This heavy contact loss will greatly increase the interface resistance and ultimately lead to premature cell failure. This is due to the rigid interface and tip effect, resulting in the formation of large dendritic flakes on the surface of the Zn anode (Figure 4c). In addition, typical two-dimensional hexagonal Zn dendrites with sharp tips are also formed in the

ZnSO_4 electrolyte (Figure S11). In contrast, the guar gum/ ZnSO_4 /glycerol system maintains a continuous and firm interfacial contact with the Zn anode after cycling, illustrating that the self-adaptive interface with the Zn anode has been built successfully by the construction of an ultrafast self-healing gel electrolyte (Figure 4d). In addition, the Zn anode after cycling also shows a flat and smooth surface (Figure 4e and Figure S12) and no obvious byproducts were detected, indicating that the uniform Zn deposition is facilitated in the guar gum/ ZnSO_4 /glycerol system. An electrochemical impedance spectroscopy (EIS) test was also conducted to evaluate the interfacial resistance for $\text{Zn}||\text{Zn}$ symmetrical cells before and after cycling (Figure S13). The charge transfer resistance of the cell with the guar gum/ ZnSO_4 /glycerol system is smaller than in the case of the guar gum/ ZnSO_4 system. After 100 cycles, the resistance increases for both electrolytes, while the resistance of the guar gum/ ZnSO_4 /glycerol system remains much lower than that of the guar gum/ ZnSO_4 system. This demonstrates that the ultrafast self-healing capability can effectively alleviate the interface issues and provide a continuous and uniform ion transport channel.

The compatibility and stability of the ultrafast self-healing electrolyte with Zn anode were evaluated using $\text{Zn}||\text{Zn}$ symmetrical cells. As illustrated in Figure S14, the $\text{Zn}||\text{Zn}$ symmetrical cell in 1 M ZnSO_4 electrolyte remains stable for 100 h with an overpotential of $\sim 40 \text{ mV}$. Due to dendrite growth, the HER, and the formation of byproducts, the time-voltage curve suddenly fluctuates in subsequent cycles and

eventually leads to cell failure. In the guar gum/ ZnSO_4 system, the $\text{Zn}||\text{Zn}$ symmetrical cell exhibits a relatively higher cycle stability for 300 h with an overpotential of ~ 50 mV. After that, there is a sudden and irreversible rise in the polarization voltage, which is ascribed to the discontinuous interfaces caused by severe Zn dendrites. In contrast, the $\text{Zn}||\text{Zn}$ symmetrical cell in the guar gum/ ZnSO_4 /glycerol system shows a stable polarization overpotential of ~ 50 mV and an ultralong life span of 1500 h, 4 times longer than that of the guar gum/ ZnSO_4 system, which also confirms the superiority of the dynamic adaptive interface. When the applied current density and cycling capacity were increased to a high current density and large capacity of 10 mA cm^{-2} and 10 mAh cm^{-2} , respectively (Figure 4f and Figure S15), the $\text{Zn}||\text{Zn}$ symmetrical cell in the guar gum/ ZnSO_4 /glycerol system remains stable for 400 h. These values are superior to those of previously reported quasi-solid electrolytes and better than those obtained in most advanced Zn-based anodes and electrolytes,^{34,40–43} reflecting the efficacy of the guar gum/ ZnSO_4 /glycerol system in suppressing Zn dendrite growth.

Finally, full cells were assembled to verify the availability and superiority of the self-adaptive interface with Zn anodes. Typically, cathode materials were prickly ball-shaped MnO_2 (Figure 5a and Figures S16 and S17). Clearly, full batteries with a self-healing electrolyte present a greatly enhanced overall electrochemical performance. The energy storage mechanism of the full batteries based on the guar gum/ ZnSO_4 /glycerol electrolytes is similar to that of the Zn/ MnO_2 battery with liquid electrolytes.⁴⁴ Cyclic voltammogram (CV) curves of the full cells in the self-healing electrolyte and pure guar gum electrolyte were examined in the range from 0.8 to 1.8 V (Figure 5b), both presenting two overlapped anodic peaks. In addition, the reduction peak at 1.25 V in self-healing electrolytes is higher than 1.22 V in pure guar gum electrolytes due to the strong interaction between electrolyte and Zn anodes, which promotes the interfacial Zn^{2+} charge transfer kinetics. In addition, in comparison with a full cell using guar gum/ ZnSO_4 electrolytes (Figure S18), the full cell with an ultrafast self-healing electrolyte has a greatly improved rate performance, attributed to the dynamic and compact interface.

With regard to the cycling performance, the quasi-solid-state Zn- MnO_2 battery with the self-healing electrolyte exhibits a discharge capacity of 200 mAh g^{-1} at 1 A g^{-1} after 500 cycles, corresponding to a capacity retention of 95% with a CE value approaching 100% (Figure 5c). In contrast, the capacity of the full cell with the guar gum/ ZnSO_4 electrolyte gradually decreased to 51.5% of the initial capacity, which is mainly ascribed to the growth of Zn dendrites and contact loss of the interface. More encouragingly, under a high current density of 10 A g^{-1} (Figure 5d), this quasi-solid-state zinc-ion cell holds 98.5% of its original capacity, again demonstrating the superiority of ultrafast capability and the self-adaptive interface. To verify its usability in practical application, the self-healing quasi-solid-state ZIBs were connected in series to power an LED device containing 51 bulbs (Figure 5e and Figure S19). When the ZIBs are cut off at the same time, the LED device is powered off immediately. Due to the superior self-healing capability, when the broken quasi-solid-state ZIBs were reconnected for 30 s, the LED device was lit up again with a negligible difference in brightness in comparison with the beginning state, further demonstrating the great potential of this battery in the sustainable development of energy storage.

In conclusion, a highly stable quasi-solid-state zinc-ion battery was constructed using an ultrafast self-healing and low solvation coordination electrolyte to realize a robust interface and a dendrite-free Zn anode. Glycerol is introduced as a second network into the guar gum based electrolyte, resulting in an effective steric molecular combing effect, which can inhibit intramolecular rotation and straighten molecular chains, thereby exposing more active sites of alcoholic hydroxyl groups. Utilizing the steric molecular combing effect of glycerol can increase the self-healing ability and modulate the solvation structure of Zn^{2+} , which could be proved by FTIR, NMR, and MD simulation results. Due to its ultrafast self-healing and the resultant self-adaptability performance, the gel electrolyte and the Zn anode maintain a continuous and close connection in dynamic during the repeated Zn stripping/plating process. Benefiting from the boosted Zn reversibility, the $\text{Zn}||\text{Zn}$ symmetric cells remain stable for more than 400 h at a current density of 10 mA cm^{-2} and a large capacity of 10 mAh cm^{-2} . The full batteries using the self-adaptive interface show a capacity of 200 mAh g^{-1} after 500 cycles at 1 A g^{-1} and deliver a high cycling performance of 98.5% capacity retention after 10000 cycles at 10 A g^{-1} . This quasi-solid-state battery sufficiently evidences the feasibility of the dynamic self-adaptive interface and paves the way for practical applications of safe energy storage devices.

■ ASSOCIATED CONTENT

Supporting Information

The Supporting Information is available free of charge at <https://pubs.acs.org/doi/10.1021/acsenergylett.2c01459>.

Experimental section, MD simulation results and DFT simulation results, schematic diagram of the electrolyte and the dendrite growth process, additional characterization of the material (XRD patterns, SEM images, optical images, XPS spectra, FTIR spectra, water-locking capacity test), additional electrochemical data (EIS profiles, Zn plating/stripping performance in symmetric cells, the rate performance of the full battery), and optical image of the self-healing Zn- MnO_2 pouch cell (PDF)

■ AUTHOR INFORMATION

Corresponding Authors

Lin Xu – State Key Laboratory of Advanced Technology for Materials Synthesis and Processing, School of Materials Science and Engineering, Wuhan University of Technology, Wuhan 430070 Hubei, People's Republic of China; Foshan Xianhu Laboratory of the Advanced Energy Science and Technology Guangdong Laboratory, Xianhu Hydrogen Valley, Foshan 528200 Guangdong, People's Republic of China; orcid.org/0000-0003-2347-288X; Email: linxu@whut.edu.cn

Liqiang Mai – State Key Laboratory of Advanced Technology for Materials Synthesis and Processing, School of Materials Science and Engineering, Wuhan University of Technology, Wuhan 430070 Hubei, People's Republic of China; Foshan Xianhu Laboratory of the Advanced Energy Science and Technology Guangdong Laboratory, Xianhu Hydrogen Valley, Foshan 528200 Guangdong, People's Republic of China; orcid.org/0000-0003-4259-7725; Email: mlq518@whut.edu.cn

Authors

Qin Liu – State Key Laboratory of Advanced Technology for Materials Synthesis and Processing, School of Materials Science and Engineering, Wuhan University of Technology, Wuhan 430070 Hubei, People's Republic of China

Renpeng Chen – State Key Laboratory of Advanced Technology for Materials Synthesis and Processing, School of Materials Science and Engineering, Wuhan University of Technology, Wuhan 430070 Hubei, People's Republic of China

Yu Liu – State Key Laboratory of Advanced Technology for Materials Synthesis and Processing, School of Materials Science and Engineering, Wuhan University of Technology, Wuhan 430070 Hubei, People's Republic of China

Yuhang Dai – State Key Laboratory of Advanced Technology for Materials Synthesis and Processing, School of Materials Science and Engineering, Wuhan University of Technology, Wuhan 430070 Hubei, People's Republic of China

Meng Huang – State Key Laboratory of Advanced Technology for Materials Synthesis and Processing, School of Materials Science and Engineering, Wuhan University of Technology, Wuhan 430070 Hubei, People's Republic of China

Complete contact information is available at:

<https://pubs.acs.org/10.1021/acseenergylett.2c01459>

Notes

The authors declare no competing financial interest.

ACKNOWLEDGMENTS

This work was supported by the National Key Research and Development Program of China (2020YFA0715000), the National Natural Science Foundation of China (51802239, 52127816), the Key Research and Development Program of Hubei Province (2021BAA070), the Foshan Xianhu Laboratory of the Advanced Energy Science and Technology Guangdong Laboratory (XHT2020-005), and the Fundamental Research Funds for the Central Universities (2020III011GX, 2020IVB057, 2019IVB054, and 2019III062JL).

REFERENCES

- (1) Bishop, M.; Shahid, N.; Yang, J.; Barron, A. R. Determination of the mode and efficacy of the cross-linking of guar by borate using MAS 11B NMR of borate cross-linked guar in combination with solution 11B NMR of model systems. *Dalton Trans.* **2004**, *17*, 2621–2634.
- (2) Sun, C.; Boluk, Y. Rheological behavior and particle suspension capability of guar gum: sodium tetraborate decahydrate gels containing cellulose nanofibrils. *Cellulose* **2016**, *23*, 3013–3022.
- (3) Liu, K.; Kang, Y.; Wang, Z.; Zhang, X. Reversible and adaptive functional supramolecular materials: "Noncovalent interaction" matters. *Adv. Mater.* **2013**, *25*, 5530–5548.
- (4) Mai, W.; Yu, Q.; Han, C.; Kang, F.; Li, B. Self-healing materials for energy-storage devices. *Adv. Funct. Mater.* **2020**, *30*, 1909912.
- (5) Zammali, M.; Liu, S.; Yu, W. Symmetry breakdown in the sol-gel transition of a Guar gum transient physical network. *Carbohydr. Polym.* **2021**, *258*, 117689.
- (6) Tee, C. K.; Wang, C.; Allen, R.; Bao, Z. An electrically and mechanically self-healing composite with pressure and flexion-sensitive properties for electronic skin applications. *Nat. Nanotechnol.* **2012**, *7*, 825–832.
- (7) Boland, C. S.; Khan, U.; Ryan, G.; Barwich, S.; Charifou, R.; Harvey, A.; Backes, C.; Li, Z.; Ferreira, M. S.; Mobius, M. E.; et al.

Sensitive electromechanical sensors using viscoelastic graphene-polymer nanocomposites. *Science* **2016**, *354*, 1257.

(8) Jiang, Y.; Shao, H. B.; Li, C. X.; Xu, T.; Zhao, Y.; Shi, G. Q.; Jiang, L.; Qu, L. T. Versatile graphene oxide putty-like material. *Adv. Mater.* **2016**, *28*, 10287.

(9) Kuang, X.; Roach, D. J.; Wu, J.; Hamel, C. M.; Ding, Z.; Wang, T.; Dunn, M. L.; Qi, H. J. Advances in 4D printing: materials and applications. *Adv. Funct. Mater.* **2019**, *29*, 1805290.

(10) Wu, H.; Yu, G.; Pan, L.; Liu, N.; McDowell, M. T.; Bao, Z.; Cui, Y. Stable Li-ion battery anodes by in-situ polymerization of conducting hydrogel to conformally coat silicon nanoparticles. *Nat. Commun.* **2013**, *4*, 1943.

(11) Li, H.; Liu, Z.; Liang, G.; Huang, Y.; Huang, Y.; Zhu, M.; Pei, Z.; Xue, Q.; Tang, Z.; Wang, Y.; Li, B.; Zhi, C. Waterproof and tailorable elastic rechargeable zinc ion batteries by a cross-linked polyacrylamide electrolyte. *ACS Nano* **2018**, *12*, 3140.

(12) Wan, F.; Zhang, L. L.; Dai, X.; Wang, X. Y.; Niu, Z. Q.; Chen, J. Aqueous rechargeable zinc/sodium vanadate batteries with enhanced performance from simultaneous insertion of dual carriers. *Nat. Commun.* **2018**, *9*, 1656.

(13) Zheng, J. X.; Zhao, Q.; Tang, T.; Yin, J. F.; Quilty, C. D.; Renderos, G. D.; Liu, X. T.; Deng, Y.; Wang, L.; Bock, D. C.; et al. Reversible epitaxial electrodeposition of metals in battery anodes. *Science* **2019**, *366*, 645–648.

(14) Wang, M.; Meng, Y.; Li, K.; Ahmad, T.; Chen, N.; Xu, Y.; Sun, J.; Chuai, M.; Zheng, X.; Yuan, Y. J. e.; et al. Toward dendrite-free and anti-corrosion Zn anodes by regulating a bismuth-based energizer. *eScience* **2022**, *1*.

(15) Wang, Z.; Zhou, M.; Qin, L.; Chen, M.; Chen, Z.; Guo, S.; Wang, L.; Fang, G.; Liang, S. Simultaneous regulation of cations and anions in an electrolyte for high-capacity, high-stability aqueous zinc-vanadium batteries. *eScience* **2022**, *2*, 209–218.

(16) Zeng, X. H.; Hao, J. N.; Wang, Z. J.; Mao, J. F.; Guo, Z. P. Recent progress and perspectives on aqueous Zn-based rechargeable batteries with mild aqueous electrolytes. *Energy Stor. Mater.* **2019**, *20*, 410–437.

(17) Bayaguud, A.; Luo, X.; Fu, Y.; Zhu, C. Cationic surfactant-type electrolyte additive enables three-dimensional dendrite-free zinc anode for stable zinc-ion batteries. *ACS Energy Lett.* **2020**, *5*, 3012–3020.

(18) Zhang, Q.; Luan, J.; Fu, L.; Wu, S.; Tang, Y.; Ji, X.; Wang, H. The three-dimensional dendrite-free zinc anode on a copper mesh with a zinc-oriented polyacrylamide electrolyte additive. *Angew. Chem., Int. Ed.* **2019**, *131*, 15988–15994.

(19) Hao, J. N.; Li, B.; Li, X. L.; Zeng, X. H.; Guo, Z. P. An in-depth study of Zn metal surface chemistry for advanced aqueous Zn-ion batteries. *Adv. Mater.* **2020**, *32*, 2003021.

(20) Yang, Y.; Liu, C. Y.; Lv, Z. H.; Yang, H.; Cheng, X.; Zhang, S. Z.; Ye, M. H.; Zhang, Y. F.; Chen, L. B.; Zhao, J. B.; et al. Redistributing Zn-ion flux by interlayer ion channels in Mg-Al layered double hydroxide-based artificial solid electrolyte interface for ultra-stable and dendrite-free Zn metal anodes. *Energy Stor. Mater.* **2021**, *41*, 230–239.

(21) Yang, Q.; Li, Q.; Liu, Z.; Wang, D.; Guo, Y.; Li, X.; Tang, Y.; Li, H.; Dong, B.; Zhi, C. Dendrites in Zn-based batteries. *Adv. Mater.* **2020**, *32*, 2001854.

(22) Chang, Z.; He, Y.; Deng, H.; Li, X.; Wu, S.; Qiao, Y.; Wang, P.; Zhou, H. A multifunctional silly-putty nanocomposite spontaneously repairs cathode composite for advanced Li–S batteries. *Adv. Funct. Mater.* **2018**, *28*, 1804777.

(23) Liu, K.; Pei, A.; Lee, H. R.; Kong, B.; Liu, N.; Lin, D. C.; Liu, Y. Y.; Liu, C.; Hsu, P. C.; Bao, Z. N.; Cui, Y. Lithium metal anodes with an adaptive "solid-liquid" interfacial protective layer. *J. Am. Chem. Soc.* **2017**, *139*, 4815–4820.

(24) Li, J.; Yu, P.; Zhang, S.; Wen, Z.; Wen, Y.; Zhou, W.; Dong, X.; Liu, Y.; Liang, Y. Mild synthesis of superadhesive hydrogel electrolyte with low interfacial resistance and enhanced ionic conductivity for flexible zinc ion battery. *J. Colloid Interface Sci.* **2021**, *600*, 586–593.

(25) Bayaguud, A.; Fu, Y.; Zhu, C. Interfacial parasitic reactions of zinc anodes in zinc ion batteries: Underestimated corrosion and hydrogen evolution reactions and their suppression strategies. *J. Energy Chem.* **2021**, *64*, 247.

(26) Jin, X.; Song, L.; Dai, C.; Ma, H.; Xiao, Y.; Zhang, X.; Han, Y.; Zhang, Z.; Duan, L.; Qu, L.; et al. A self-healing zinc ion battery under $-20\text{ }^{\circ}\text{C}$. *Energy Stor. Mater.* **2022**, *44*, 517–526.

(27) Xu, W.; Zhao, K.; Huo, W.; Wang, Y.; Wang, X.; et al. Diethyl ether as self-healing electrolyte additive enabled long-life rechargeable aqueous zinc ion batteries. *Nano Energy* **2019**, *62*, 275–281.

(28) Qiu, H.; Du, X.; Zhao, J.; Wang, Y.; Cui, G. Zinc anode-compatible in-situ solid electrolyte interphase via cation solvation modulation. *Nat. Commun.* **2019**, *10*, 5374.

(29) Hong, Z.; Ahmad, Z.; Viswanathan, V. Design principles for dendrite suppression with porous polymer/aqueous solution hybrid electrolyte for Zn metal anodes. *ACS Energy Lett.* **2020**, *5*, 2466–2474.

(30) Wang, Z.; Hu, J.; Han, L.; Wang, Z.; Wang, H.; Zhao, Q.; Liu, J.; Pan, F. A MOF-based single-ion Zn^{2+} solid electrolyte leading to dendrite-free rechargeable Zn batteries. *Nano energy* **2019**, *56*, 92–99.

(31) Liu, Z. X.; Yang, Q.; Wang, D. H.; Liang, G. J.; Zhu, Y. H.; Mo, F. N.; Huang, Z. D.; Li, X. L.; Ma, L. T.; Tang, T. C.; Zhi, C. Y. A flexible solid-state aqueous zinc hybrid battery with flat and high-voltage discharge plateau. *Adv. Energy Mater.* **2019**, *9*, 1902473.

(32) Li, C.; Zhang, Q.; Sun, J.; Li, T.; Songfeng, E.; Zhu, Z.; He, B.; Zhou, Z.; Li, Q.; Yao, Y. High performance quasi-solid-state flexible aqueous rechargeable Ag-Zn battery based on metal-organic-framework derived Ag nanowires. *ACS Energy Letters* **2018**, *3*, 2761–2768.

(33) Liu, Q.; Zhou, D.; Shanmukaraj, D.; Li, P.; Wang, G.; et al. Self-healing janus interfaces for high-performance LAGP-based lithium metal batteries. *ACS Energy Lett.* **2020**, *5*, 1456–1464.

(34) Huang, S.; Wan, F.; Bi, S.; Zhu, J.; Niu, Z.; Chen, J. A self-healing integrated all-in-one zinc-ion battery. *Angew. Chem., Int. Ed.* **2019**, *58*, 4313–4317.

(35) Luo, F.; Sun, T. L.; Nakajima, T.; Kurokawa, T.; Zhao, Y.; Sato, K.; Ihsan, A. B.; Li, X.; Guo, H.; Gong, J. P. Oppositely charged polyelectrolytes form tough, self-healing, and rebuildable hydrogels. *Adv. Mater.* **2015**, *27*, 2722–2727.

(36) Cao, Y.; Morrissey, T. G.; Acome, E.; Allec, S. I.; Wong, B. M.; Keplinger, C.; Wang, C. A Transparent, self-healing, highly stretchable ionic conductor. *Adv. Mater.* **2017**, *29*, 1605099.

(37) Jaumaux, P.; Liu, Q.; Zhou, D.; Xu, X.; Wang, T.; Wang, Y.; Kang, F.; Li, B.; Wang, G. Deep-eutectic-solvent-based self-healing polymer electrolyte for safe and long-life lithium-metal batteries. *Angew. Chem., Int. Ed.* **2020**, *59*, 9134–9142.

(38) Sinton, S. W. Complexation chemistry of sodium borate with poly(vinyl alcohol) and small diols. A ^{11}B NMR Study. *Macromolecules* **1987**, *20*, 2430–2441.

(39) Schultz, R. K.; Myers, R. R. The chemorheology of poly(vinyl alcohol)-borate gels. *Macromolecules* **1969**, *2*, 281–285.

(40) Zhang, M.; Yu, P.; Xiong, K.; Wang, Y.; Liu, Y.; Liang, Y. Construction of mixed ionic-electronic conducting scaffolds in Zn powder: A Scalable Route to Dendrite-Free and Flexible Zn Anodes. *Adv. Mater.* **2022**, *34*, 2200860.

(41) Li, Z.; Chen, D.; An, Y.; Chen, C.; Wu, L.; Chen, Z.; Sun, Y.; Zhang, X. Flexible and anti-freezing quasi-solid-state zinc ion hybrid supercapacitors based on pencil shavings derived porous carbon. *Energy Stor. Mater.* **2020**, *28*, 307–314.

(42) Cao, L.; Li, D.; Hu, E.; Xu, J.; Deng, T.; Ma, L.; Wang, Y.; Yang, X. Q.; Wang, C. Solvation structure design for aqueous Zn metal batteries. *J. Am. Chem. Soc.* **2020**, *142*, 21404–21409.

(43) Sun, P.; Ma, L.; Zhou, W.; Qiu, M.; Wang, Z.; Chao, D.; Mai, W. Simultaneous Regulation on solvation shell and electrode interface for dendrite-free Zn ion batteries achieved by a low-cost glucose additive. *Angew. Chem., Int. Ed.* **2021**, *60*, 18247–18255.

(44) Zhang, N.; Cheng, F. Y.; Liu, J. X.; Wang, L. B.; Long, X. H.; Liu, X. S.; Li, F. J.; Chen, J. Rechargeable aqueous zinc-manganese dioxide batteries with high energy and power densities. *Nat. Commun.* **2017**, *8*, 405.

Recommended by ACS

Localized Hydrophobicity in Aqueous Zinc Electrolytes Improves Zinc Metal Reversibility

Peichao Zou, Huolin L. Xin, et al.

SEPTEMBER 07, 2022
NANO LETTERS

READ 

Working Aqueous Zn Metal Batteries at $100\text{ }^{\circ}\text{C}$

Jiawei Wang, Hua Wang, et al.

SEPTEMBER 06, 2022
ACS NANO

READ 

Crystal Water Boosted Zn^{2+} Transfer Kinetics in Artificial Solid Electrolyte Interphase for High-Rate and Durable Zn Anodes

Hongrun Jin, Liang Huang, et al.

AUGUST 24, 2022
ACS APPLIED ENERGY MATERIALS

READ 

Aqueous Electrolytes with Hydrophobic Organic Cosolvents for Stabilizing Zinc Metal Anodes

Licheng Miao, Ning Zhang, et al.

MAY 27, 2022
ACS NANO

READ 

Get More Suggestions >